Chinese Chemical Letters 34 (2023) 107766

Contents lists available at ScienceDirect

Chinese Chemical Letters

journal homepage: www.elsevier.com/locate/cclet

Ce-doped MIL-125-NH_2 coupled Ce^{4+}/Ce^{3+} and Ti^{4+}/Ti^{3+} redox mediators for thermo-enhanced photocatalytic oxidative desulfurization

Kaiyue Zhang[a], Feng Chu[a], Yezi Hu[b], Xiubing Huang[a,*], Guixia Zhao[b,*], Ge Wang[a,*]

[a] Beijing Key Laboratory of Function Materials for Molecule & Structure Construction, School of Materials Science and Engineering, University of Science and Technology Beijing, Beijing 100083, China
[b] College of Environmental Science and Engineering, North China Electric Power University, Beijing 102206, China

ARTICLE INFO

Article history:
Received 10 May 2022
Revised 10 August 2022
Accepted 20 August 2022
Available online 22 August 2022

Keywords:
Photocatalytic oxidative desulfurization
Ce-doped-MIL-125-NH_2
Ce^{4+}/Ce^{3+} and Ti^{4+}/Ti^{3+} redox couples
Thermal enhancement
Visible light
Photocatalytic oxidation

ABSTRACT

Photocatalytic oxidative desulfurization (PODS) over efficient earth-abundant catalysts to obtain clean fuel oil is of great importance for the environmental protection. In this work, a series of Ce-doped MIL-125-NH_2 photocatalysts were successfully prepared *via* a simple *in-situ* doping method and exhibited superior PODS performance of dibenzothiophene (DBT) under mild reaction conditions. The 1.0 mol% Ce/MIL-125-NH_2 catalyst achieved 100% sulfur removal within 22 min at 30 °C under visible light illumination, which is mainly attributed to the high surface area and the formation of Ce-Ti-oxo clusters due to electronic coupling. The valence transformation of Ce^{4+}/Ce^{3+} and Ti^{4+}/Ti^{3+} redox mediators could not only expose abundant Lewis acid sites, but also promote the separation and transfer of photogenerated charges. In addition, increasing the reaction temperature has been demonstrated to be effective in promoting the PODS performance. Additionally, a thermo-enhanced PODS mechanism was proposed over Ce/MIL-125-NH_2, demonstrating the great potential of thermal energy to promote the desulfurization activity.

A large amount of SO_x compounds is released due to the combustion of fuel oil, causing serious environmental pollution and ecological damage. Recently, deep desulfurization of petroleum products to produce clean fuels is receiving extensive attention [1]. The conventional industrial hydrodesulfurization requires high temperature and pressure harsh reaction conditions, which is ineffective to heterocyclic sulfur compounds such as the dibenzothiophene (DBT) and its derivatives [2]. Up to now, several strategies have been reported for desulfurization of sulfur compounds, such as oxidative desulfurization [3,4], photocatalytic oxidative desulfurization [5], and physical adsorptive desulphurization [6]. Among these strategies, photocatalytic oxidative desulfurization (PODS) has been attracting increasing attention and been widely studied due to its high efficiency and low cost for the removal of heterocyclic sulfur compounds and their derivates under mild operating conditions [7]. However, the current desulfurization photocatalysts, such as Ag-TiO_2 [8], Ti_3C_2/g-C_3N_4 [9,10], CeO_2 [11] and heteropoly-acid (HPA) [12], are still disadvantaged due to their poor light absorption, fast recombination of photogenerated carriers, and poor structural modification, which cannot achieve satisfactory and efficient deep desulfurization performance [13].

Metal-organic frameworks (MOFs), as novel porous structural materials, possess large surface area and abundant unsaturated sites and easy-tailored structure [14,15], which are favorable to adsorption and oxidation performance of sulfur compounds [16–18]. Especially, Ti-based MOFs exhibit certain oxidative desulfurization performance at 60 °C [19,20]. So far PODS using pristine MOFs is rarely reported because of the unsatisfactory visible-light responsiveness and limited active sites as well as ambiguous reaction mechanism. Semiconductor modification and metal doping to modify MOFs are effective strategies to improve the photo-response ability and photocatalytic activity. Bagheri *et al.* constructed MoO_3-MOF hybrid photocatalysts and exhibited excellent photocatalytic desulfurization performance due to the synergic effects of the active surface of MOFs together with active center of MoO_3 under UV and visible light irradiation [21]. The construction of hetero-structure not only improves photoexicited electron behavior, but also enhance catalytic activity [22,23]. Besides constructing heterojunction strategy, defect engineering *via* metal ion doping draws tremendous attention to expose more active sites and modulate electron interaction [24,25]. The incorporation of doping Ce with high abundance, low cost and inher-

* Corresponding authors.
E-mail addresses: xiubinghuang@ustb.edu.cn (X. Huang), guixiazhao@ncepu.edu.cn (G. Zhao), gewang@ustb.edu.cn (G. Wang).

https://doi.org/10.1016/j.cclet.2022.107766
1001-8417/

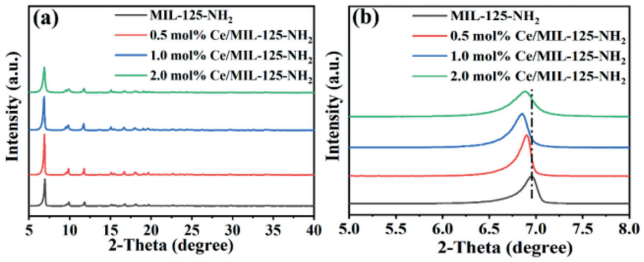

Fig. 1. (a) XRD patterns and (b) partial enlarged patterns of XRD of MIL-125-NH_2 and 0.5 mol%, 1.0 mol%, and 2.0 mol% Ce/MIL-125-NH_2.

ent Ce^{4+}/Ce^{3+} redox pairs into pristine MOFs has been widely investigated. For example, Ebrahim *et al.* prepared Ce(III) doped Zr-based MOFs to exhibit excellent NO_2 adsorption at ambient conditions [26]. Yang *et al.* synthesized Ce ion-implanted MIL-96 *via* incipient wetness impregnation for high-efficiency removing fluoride from water [27]. The Ce^{4+}/Ce^{3+} redox cycling might also endow MOFs with attractive adsorptive performance. Zhang *et al.* developed Ti-doped UiO-66(Ce) *via* cation-exchange method to improve the photocatalytic reduction performance, in which Ti mediator species induced abundant oxygen vacancies and active radicals ($O_2^{\bullet-}$ and $^{\bullet}OH$) as well as enhanced photoelectronic generation and transfer [28]. Patrycja *et al.* reported novel Ti-substituted (Ce)UiO-X MOFs@TiO_2 heterojunction to exhibit outstanding photocatalytic performance due to the synergistic effect of Ce-Ti species including reversible Ce^{4+}/Ce^{3+} and Ti^{4+}/Ti^{3+} redox mediators and the incorporation of TiO_2 [29]. However, utilizing metal-doped MOFs with longer-lived excited states and effective charge separation as photocatalyst for the PODS of the sulfur compound from light oil has been rarely exploited.

In this work, Ce-doped MIL-125-NH_2 samples (Ce/MIL-125-NH_2) with controlled Ce-doping content were systematically investigated for the photocatalytic oxidation of DBT. The experimental results show that appropriate Ce doping improves the separation efficiency of photo-generated carriers under visible light, thereby achieving the excellent conversion of DBT. In addition, the reaction temperature significantly enhanced the PODS performance. Finally, a thermo-enhanced PODS mechanism was explored through radical trapping experiment and control experiments.

The structures of as-synthesized Ce/MIL-125-NH_2 composites were revealed by XRD analysis. As presented in Fig. 1, the main diffraction peaks of MIL-125-NH_2 with good crystallinity are consistent with the XRD pattern of our previous report [30], which proves the successful configuration. Meanwhile, the XRD patterns of Ce-doped MIL-125-NH_2 samples are basically similar to that of MIL-125-NH_2. But the diffraction peak at 6.9 ° shifts to a lower angle due to the larger radius of Ce^{3+} (1.034 Å) than Ti^{4+} (0.68 Å) (Fig. 1b). The shift offset is greater with the increased Ce doping content, indicating that the Ce species are successfully doped into the MIL-125-NH_2 lattice without significantly affecting the crystal structure and crystallinity.

As shown in Fig. S1 (Supporting information), the morphology of the sample was characterized by SEM. MIL-125-NH_2 is disc-shaped with a diameter of 700-800 nm and a thickness of 200-300 nm. But the diameter and thickness of all the Ce-doped samples decrease sequentially. 2.0 mol% Ce/MIL-125-NH_2 has a diameter of 300-600 nm and a thickness of 50-60 nm. The doped Ce inhibits the growth of MIL-125-NH_2 or disturbs the interactions between the Ti-metallic centers and the organic ligands [26]. In addition, EDS spectra of 1.0 mol% Ce/MIL-125-NH_2 in Fig. S1e also indicate that Ce^{3+} is uniformly doped into the framework of MIL-125-NH_2.

The FT-IR spectra was used to confirm the bond structure of MIL-125-NH_2 (Fig. S2a in Supporting information). The peak at 3418 cm^{-1} is related to the stretching vibration of the O-H bond. The strong absorption peak at 1648 cm^{-1} is the characteristic peak of the carbonyl functional group in the O–C=O structure. The peak at 1391 cm^{-1} is attributed to the C-N bond between the carbon atom connecting the benzene ring and the nitrogen atom on the amino group, while the peaks in the range of 540-800 cm^{-1} belong to the stretching vibration of the O-Ti-O bond [31,32]. The incorporation of Ce does not induce new absorption peaks, which indicates that the Ce-doped MIL-125-NH_2 maintains the original framework structure. As shown in Fig. S2b (Supporting information), the MIL-125-NH_2 and Ce/MIL-125-NH_2 samples demonstrate a typical type I curve. The specific surface areas of MIL-125-NH_2, 0.5 mol%, 1.0 mol% and 2.0 mol% Ce/MIL-125-NH_2 are 1274.9, 1158.3, 1213.8 and 1041.8 m^2/g, respectively, indicating that slight Ce doping does not affect the BET to a large extent, but a large amount of Ce doping would induce the partial presence of Ce retains in the pores of the MOF, causing a decrease in specific surface area. The pore size distribution curves in Fig. S2c verify the similar microporous structure between MIL-125-NH_2 and Ce/MIL-125-NH_2.

In addition, the element valence state and chemical environment of the sample were further analyzed by XPS. In the spectra of Ti 2p (Fig. S3a in Supporting information), the binding energies located at 458.8 eV and 464.5 eV are assigned to Ti $2p_{3/2}$ and Ti $2p_{1/2}$. After Ce doping, it can be observed that both two peaks are shifted to lower binding energy, indicating Ce doping increases the electron density of Ti. Moreover, two new peaks corresponding to Ti^{3+} ions appear near 459 eV and 464 eV, which can be attributed to the redistribution of charges within the system due to Ce doping. In the N 1s spectra (Fig. S3b in Supporting information), the peaks at 399.0, 400.0 and 402.5 eV correspond to pyridine N, pyrrolic N and amino N, respectively. After Ce doping, the N 1s peaks shift towards lower binding energies which are caused by the increased electron density of N. In the spectra of O 1s (Fig. S3c in Supporting information), there is a Ce-O peak at 530.5 eV for Ce/MIL-125-NH_2 samples [33], which effectively indicates the interactions of Ce with Ti-O center or the organic linker *via* π-complexation or a chelation process [26]. The spectra of Ce 3d is shown in Fig. S3d (Supporting information) where eight characteristic peaks can be observed. The peaks at 885.1 eV and 903.5 eV are attributed to Ce^{3+}, while the three pairs of peaks at 882.9 eV and 901.4 eV, 889.3 eV and 908.1 eV, and 898.9 eV and 917.2 eV are attributed to Ce^{4+} ions, indicating the coexistence of Ce^{4+} and Ce^{3+} in the Ce/MIL-125-NH_2 sample [34]. Incorporation of Ce into Ti-MOFs leads to the formation of the Ti-Ce clusters and generates abundant Ti^{3+} and Ce^{4+} on the surface. The generation of Ce^{4+}/Ce^{3+} and Ti^{4+}/Ti^{3+} redox mediators promote the formation of more Lewis acid site and enhances the photo-oxidation ability. Determined by the ICP-AES measurements of Ce/MIL-125-NH_2 in Table S1 (Supporting information), the actual amounts of Ce are calculated to be 0.73 mol%, 1.46 mol%, and 2.92 mol% for 0.5 mol%, 1.0 mol% and 2.0 mol% Ce/MIL-125-NH_2, respectively.

In order to explore the effect of Ce incorporation on the optical behavior, the photo-response properties and band structure of MIL-125-NH_2 and Ce/MIL-125-NH_2 were examined by UV-vis spectroscopy and Mott Schottky plots. It can be seen from Fig. S4a (Supporting information) that the absorption edge of MIL-125-NH_2 is about 500 nm, and the visible-light absorption range is slightly red-shifted after doping with Ce. The results indicate the doping of Ce can slightly broaden the visible light absorption range. The estimated band gaps of MIL-125-NH_2, 0.5 mol%, 1.0 mol%, and 2.0 mol% Ce/MIL-125-NH_2 are 2.32 eV, 2.31 eV, 2.30 eV and 2.29 eV, respectively. The Mott-Schottky plots in Fig. S5a (Supporting information) were measured to indicate the n-type semiconductor and the corresponding flat band potentials of MIL-125-NH_2 and 1.0 mol% Ce/MIL-125-NH_2 (−1.15 and −0.89 V *vs.* Ag/AgCl). Therefore,

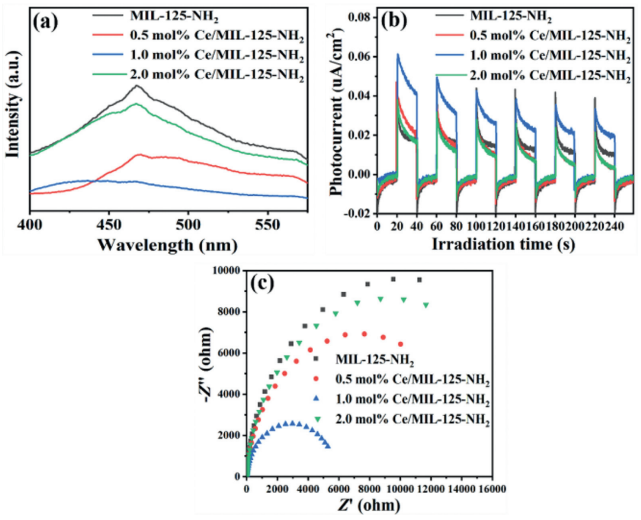

Fig. 2. (a) PL spectra, (b) transient photocurrent response and (c) EIS Nyquist plots of MIL-125-NH_2 and Ce/MIL-125-NH_2.

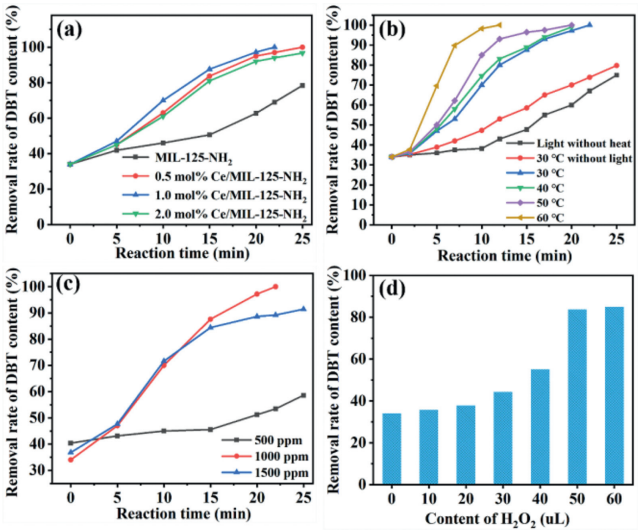

Fig. 3. (a) Photocatalytic DBT desulfurization rate of MIL-125-NH_2 and Ce/MIL-125-NH_2 at 30 °C. (b) DBT desulfurization of 1.0 mol% Ce/MIL-125-NH_2 sample at different temperatures. (c) The effect of different DBT concentrations on the photocatalytic DBT desulfurization performance at 30 °C. (d) The desulfurization effect of 1.0 mol% Ce/MIL-125-NH_2 catalyst under different H_2O_2 additions.

combined with band gap, the conduction band (CB) and valence band (VB) were calculated, as shown in Fig. S5b. In order to further verify that the Ce doping facilitates the separation and transfer efficiency of photogenerated carriers, photoluminescence (PL) spectroscopy was performed. As shown in Fig. 2a, the 1.0 mol% Ce/MIL-125-NH_2 sample has the lowest peak intensity at the excitation wavelength of 350 nm. In addition, as observed in Figs. 2b and c, 1.0 mol% Ce/MIL-125-NH_2 has the highest photocurrent density and the smallest charge transfer resistance, indicating that appropriate amount of Ce doping has stronger photo-excited carrier separation and transfer ability under visible light, which is conducive to improving the photocatalytic performance effectively [35].

To investigate the photocatalytic properties of Ce-doped MIL-125-NH_2, the PODS of DBT was firstly carried out under visible light irradiation at 30 °C. As shown in Fig. 3a, the DBT extraction rate is 34% at the beginning of the reaction due to the addition of acetonitrile. Acetonitrile plays two important roles in the

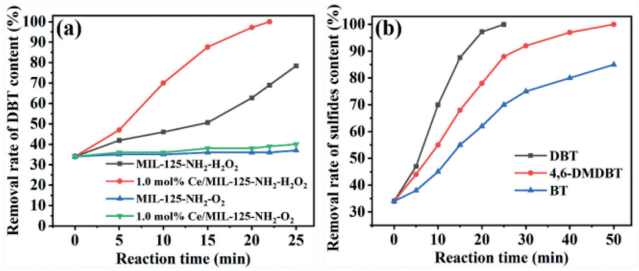

Fig. 4. (a) Photocatalytic DBT desulfurization rate of MIL-125-NH_2 and 1.0 mol% Ce/MIL-125-NH_2 at O_2 atmosphere. (b) Removal of different sulfur-containing substrates. Reaction conditions: $T = 30$ °C, $m_{catal} = 10$ mg, $V_{oil} = 5$ mL, initial S content = 1000 ppm, and $V_{H_2O_2} = 50$ μL.

system. On the one hand, the catalyst was uniformly dispersed in this solution to avoid sticking to the wall during the reaction. On the other hand, the acetonitrile acts as an extractant of substrate DBT to contact well with the catalyst. In Fig. 3a, 1.0 mol% Ce/MIL-125-NH_2 has a 100% removal rate of DBT within 22 min at 30 °C while it is only 69% for MIL-125-NH_2. The enhanced performance is largely due to the existence of Ce^{4+}/Ce^{3+} and Ti^{4+}/Ti^{3+} redox mediators, which would promote the separation of photo-induced charge carriers, the generation of more Lewis acid sites and the decomposition of H_2O_2. In order to deeply investigate the effect of temperature and light, 1.0 mol% Ce/MIL-125-NH_2 was tested at different temperatures (*e.g.*, 30 °C, 40 °C, 50 °C and 60 °C) with or without visible light irradiation, respectively. As shown in Fig. 3b, the temperature significantly improves the oxidative removal rate of DBT, especially, the heat-driven effect is extremely obvious at 2-10 min. Furthermore, increasing the reaction temperature accelerates the reaction rate [36,37]. Particularly, the oxidative desulfurization rate reaches 100% only within 12 min at 60 °C, indicating the positive synergistic effect of light and heat in the oxidative removal of DBT. However, only 75% and 80% removal rates are obtained with only light irradiation and without light irradiation at 30 °C after 25 min respectively. In addition, the effect of the initial DBT concentration was discussed for the 1.0 mol% Ce/MIL-125-NH_2 sample under the same O/S ratio, as shown in Fig. 3c. The results show that the 1000 ppm DBT is the optimal initial concentration, while the poor oxidation efficiency of DBT at 500 ppm concentration is attributed to the low concentration of active radicals generated by insufficient H_2O_2 content. The decrease in photocatalytic activity at higher DBT concentrations may be due to the high substrate content [38]. The PODS with different H_2O_2 content in 1000 ppm DBT concentration was performed to further investigate the effect of O/S molar ratio. As shown in Fig. 3d, the desulfurization rate gradually increases with the increase of H_2O_2 content within a certain range. The excessive H_2O_2 amount leads to negligible improvement because too excessive oxidant cannot be effectively activated by photocatalysts. When 50 uL H_2O_2 (O/S = 5) was added to the system, the best desulfurization performance was obtained under 15 min illumination at 30 °C, demonstrating the important role of the O/S molar ratio in PODS. In addition, PODS over Ce-doped MIL-125-NH_2 at O_2 atmosphere was performed. The results in Fig. 4a indicate the reaction hardly proceeds under oxygen atmosphere, demonstrating the crucial role of H_2O_2 as active radical initiator in photocatalytic oxidative desulfurization.

To explore the general utilization of Ce-doped MIL-125-NH_2 catalysts, the thermo-assisted photocatalytic oxidation of other typical aromatic sulfides, such as benzothiophene (BT) and 4,6-dimethyldibenzothiophene (4,6-DMDBT), were carried out to prove the universality of the prepared catalysts under the same condition (Fig. 4b). The sulfur removal efficiency of 4,6-DMDBT reached 100%, and BT can reach 85% under visible light irradiation at 30 °C.

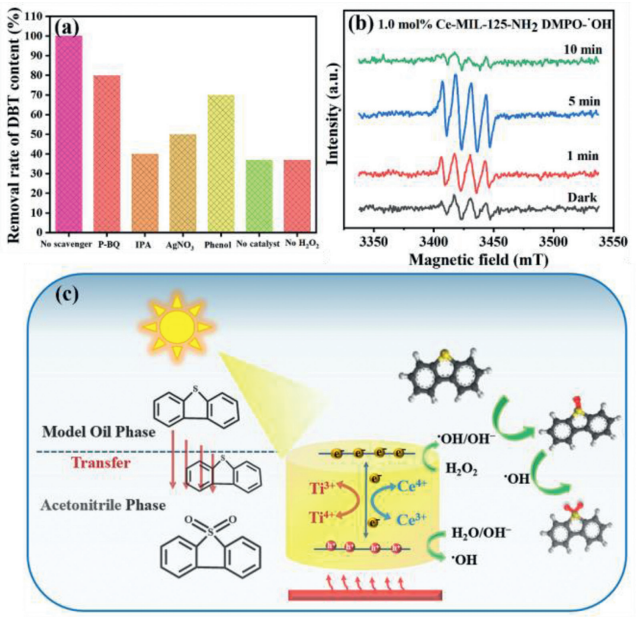

Fig. 5. (a) Effect of adding different scavengers on photocatalytic oxidation of DBT with 1.0 mol% Ce/MIL-125-NH_2. (b) ESR spectra of 1.0 mol% Ce/MIL-125-NH_2 under dark and different time illumination. (c) Proposed mechanism of photocatalytic oxidation of DBT on Ce/MIL-125-NH_2.

Due to the presence of steric hindrance effect and electron density of the sulfur atom, the order of reactivity is DBT > 4,6-DMDBT > BT [39]. The sequence of S electron densities is 4,6-DMDBT > DBT > BT, high S electron density is conducive to electrophilic addition reaction. However, due to the steric hindrance effect, 4,6-DMDBT with two methyl groups has lower desulfurization performance than DBT. Hence, the as-prepared catalyst has the potential application value for practical desulfurization. To evaluate the recycling stability of 1.0 mol% Ce/MIL-125-NH_2, the reacted catalysts were collected by centrifugation, washed and dried overnight at 80 °C, and subjected to DBT desulfurization experiments under the same reaction conditions. As shown in Fig. S6a (Supporting information), the slightly decreased desulfurization rate may be due to the catalyst loss or the residual organic adsorbed within the pores of Ce/MIL-125-NH_2 even though the XRD patterns and SEM images in Figs. S6b and c (Supporting information) are consistent before and after cycling. As shown in Fig. S7 (Supporting information), the FT-IR and UV-vis spectra of 1.0 mol% Ce/MIL-125-NH_2 before and after cycling are different, indicating the possible adsorption of residual sulfur compounds. The similar BET area (1213.8 m^2/g *vs.* 1251.7 m^2/g) and the decreased pore volume (0.804 cc/g *vs.* 0.522 cc/g) indicate that pores of 1.0 mol% Ce/MIL-125-NH_2 may be blocked by the residual sulfur compounds. The presence of mesopores structure in Fig. S7d is attributed that H_2O_2 addition probably destroyed pore structure.

In order to explore the PODS mechanism of DBT, radical trapping experiments were performed to clarify the active radicals. p-Benzoquinone (P-BQ), *tert*-butanol (IPA), phenol and silver nitrate ($AgNO_3$) can act as scavengers for superoxide radicals ($O_2^{\bullet-}$), hydroxyl radicals ($^{\bullet}OH$), hole (h^+) and electron (e^-), respectively. As shown in Fig. 5a, the addition of IPA significantly inhibits the DBT oxidation efficiency, proving $^{\bullet}OH$ is the main radicals. It is clear from Figs. 4a and 5a that $O_2^{\bullet-}$ is not dominant reactive radical. The addition of phenol and $AgNO_3$ scavengers could decrease the sulfur removal, indicating h^+ and e^- may participate in the reaction. In addition, only about 37% extraction rate is achieved without catalyst or H_2O_2, demonstrating the important roles of catalyst and H_2O_2 during the oxidative desulfurization process. ESR tests were also performed on MIL-125-NH_2 and 1.0 mol% Ce/MIL-125-NH_2 to further verify the presence of $^{\bullet}OH$. As shown in Fig. S8 (Supporting information) and Fig. 5b, H_2O_2 partially decomposes into $^{\bullet}OH$ in the dark, and $^{\bullet}OH$ is generated at a faster rate with the involvement of visible light irradiation, leading to a faster reaction rate. It can be also seen that H_2O_2 can be decomposed faster in the 1.0 mol% Ce/MIL-125-NH_2 system than in MIL-125-NH_2, demonstrating the doped Ce facilitates the decomposition of H_2O_2.

In order to illustrate the conversion pathway of DBT in the extraction-PODS system, the collected acetonitrile liquid after 10 min and 20 min reaction was detected by GC-MS (Fig. S9 in Supporting information). After 10 min illumination, the DBT and $DBTO_2$ were detected in acetonitrile phase, while only $DBTO_2$ was detected after 20 min, indicating that there was obvious transfer behavior of DBT molecules between the oil phase and the acetonitrile phase [40]. During the reaction process, the acetonitrile phase extracts DBT in model oil to reach the extraction-dissolution equilibrium, and the product $DBTO_2$ is also soluble in the acetonitrile phase. Fig. 5c illustrates vividly the PODS process. The reaction process consists of two steps. Firstly, DBT molecules are rapidly extracted from the oil phase to the acetonitrile phase. Secondly, H_2O_2 partially decomposes into $^{\bullet}OH$ *via* photogenerated electrons under visible light illumination. And the photogenerated holes react with water or OH^- to generate $^{\bullet}OH$. Finally, the adsorbed DBT is oxidized to $DBTO_2$ [29,41,42].

Summarily, Ce-doped MIL-125-NH_2 samples with different Ce-doping content were investigated as photocatalysts for the PODS performance of DBT under mild reaction conditions. Particularly, the desulfurization rate of DBT over 1.0 mol% Ce/MIL-125-NH_2 reaches 100% within 22 min at 30 °C under visible light irradiation. The electron interaction between Ce-Ti species leads to the formation of Ce^{4+}/Ce^{3+} and Ti^{4+}/Ti^{3+} redox mediators, which not only increase the Lewis acid sites, but also promote the separation and transfer of photogenerated electron-hole pairs, thereby realizing efficient desulfurization efficiency. The synergistic effect of external heat and visible light significantly increased the oxidative desulfurization rate. The feasible doping strategy and thermal enhancement effect will open new avenues for the design of other visible-light-responsive photocatalysts to solve environmental pollution and energy problems.

Declaration of competing interest

The authors declare that they have no known competing financial interests or personal relationships that could have appeared to influence the work reported in this paper.

Acknowledgments

This work was supported by the National Key Research and Development Program of China (No. 2021YFB3500700), the National Natural Science Foundation of China (No. 21976054), and Fundamental Research Funds for the Central Universities (No. FRF-TP-20-005A3).

Supplementary materials

Supplementary material associated with this article can be found, in the online version, at doi:10.1016/j.cclet.2022.107766.

References

[1] A. Rajendran, T. Cui, H. Fan, et al., J. Mater. Chem. A 8 (2020) 2246–2285.
[2] X. Zhou, X. Li, R. Prins, et al., J. Catal. 394 (2021) 167–180.
[3] J. Ye, J. Wen, D. Zhao, et al., Chin. Chem. Lett. 31 (2020) 2819–2824.
[4] Z. Wu, Y. Li, C. Zhang, et al., Chem. Catal. 2 (2022) 1009–1045.
[5] G. Lu, F. Chu, X. Huang, et al., Coord. Chem. Rev. 450 (2022) 214240.

[6] X. Guan, Y. Wang, W. Cai, Chin. Chem. Lett. 30 (2019) 1310–1314.
[7] M. Chi, T. Su, L. Sun, et al., Appl. Catal. B: Environ. 275 (2020) 119134.
[8] Y. Chen, C. Shen, J. Wang, G. Xiao, G. Luo, ACS Sustain. Chem. Eng. 6 (2018) 13276–13286.
[9] B. Li, H. Song, F. Han, L. Wei, Appl. Catal. B: Environ. 269 (2020) 118845.
[10] G. Zhao, S. Hao, J. Guo, et al., Chin. J. Catal. 42 (2021) 501–509.
[11] X. Li, Z. Zhang, C. Yao, et al., Appl. Surf. Sci. 364 (2016) 589–596.
[12] J. Li, Z. Yang, S. Li, et al., J. Ind. Eng. Chem. 82 (2020) 1–16.
[13] G. Zhao, X. Xu, Nanoscale 13 (2021) 10649–10667.
[14] Y. Xue, G. Zhao, R. Yang, et al., Nanoscale 13 (2021) 3911–3936.
[15] H. Zhang, Y. Yang, C. Li, et al., J. Mater. Chem. A 9 (2021) 16743–16750.
[16] I. Ahmed, S.H. Jhung, J. Hazard. Mater. 301 (2016) 259–276.
[17] B.N. Bhadra, S.H. Jhung, Appl. Catal. B: Environ. 259 (2019) 118021.
[18] X. Zhang, Z. Zhang, B. Zhang, et al., Appl. Catal. B: Environ. 256 (2019) 117804.
[19] Y. Zhang, G. Li, L. Kong, H. Lu, Fuel 219 (2018) 103–110.
[20] N. Li, Z. Zhang, J. Zhang, et al., Dalton Trans. 50 (2021) 6506–6511.
[21] M. Bagheri, M.Y. Masoomi, A. Morsali, ACS Catal. 7 (2017) 6949–6956.
[22] Y. Xing, X. Wang, S. Hao, et al., Chin. Chem. Lett. 32 (2021) 13–20.
[23] G. Zhao, Y. Xing, S. Hao, et al., Chin. Chem. Lett. 32 (2021) 277–281.
[24] G. Mo, L. Wang, J. Luo, Sep. Purif. Technol. 277 (2021) 119643.
[25] G. Zhao, W. Ma, X. Wang, et al., Adv. Powder Mater. 1 (2022) 100008.
[26] A.M. Ebrahim, T.J. Bandosz, ACS Appl. Mater. Interfaces 5 (2013) 10565–10573.
[27] X. Yang, S. Deng, F. Peng, T. Luo, Dalton Trans. 46 (2017) 1996–2006.
[28] Y. Zhang, H. Chen, Y. Pan, et al., Chem. Comm. 55 (2019) 13959–13962.
[29] P. Parnicka, W. Lisowski, T. Klimczuk, A. Mikolajczyk, A. Zaleska-Medynska, Appl. Catal. B: Environ. 310 (2022) 121349.
[30] Z. Wu, X. Huang, H. Zheng, et al., Appl. Catal. B: Environ. 224 (2018) 479–487.
[31] G. Ye, Y. Gu, W. Zhou, W. Xu, Y. Sun, ACS Catal. 10 (2020) 2384–2394.
[32] G. Lu, X. Huang, Y. Li, et al., J. Energy Chem. 43 (2020) 8–15.
[33] J. He, Y. Xu, W. Wang, et al., Chem. Eng. J. 379 (2020) 122431.
[34] X. Dong, Y. Lin, G. Ren, Y. Ma, L. Zhao, Colloid Surf. A 608 (2021) 125578.
[35] Y. Zou, Y. Hu, A. Uhrich, et al., Appl. Catal. B: Environ. 298 (2021) 120584.
[36] X. Li, K. Zhang, X. Huang, et al., Nanoscale 13 (2021) 19671–19681.
[37] K. Zhang, G. Lu, F. Chu, X. Huang, Catal. Sci. Technol. 11 (2021) 7060–7071.
[38] A. Najafidoust, S. Allahyari, N. Rahemi, M. Tasbihi, Ceram. Int. 46 (2020) 4707–4719.
[39] J. Guo, L. Chu, L. Wang, et al., Appl. Surf. Sci. 579 (2022) 152251.
[40] Y. Zhang, R. Wang, Appl. Catal. B: Environ. 234 (2018) 247–259.
[41] F. Abedini, S. Allahyari, N. Rahemi, Appl. Surf. Sci. 569 (2021) 151086.
[42] Q. Huo, G. Liu, H. Sun, et al., Chem. Eng. J. 422 (2021) 130036.